molecular pharmaceutics

Article

A Novel Model System for Understanding Anti-Cancer Activity of Hypoxia-Activated Prodrugs

Zhiyuan Sun, Haoqi Zhang, Jin Wu, Fangli Gao, Congcong Zhang, Xueyan Hu, Qiqi Liu, Yonghua Wei, Jie Zhuang, and Xinglu Huang

Mol. Pharmaceutics, **Just Accepted Manuscript** • Publication Date (Web): 30 Apr 2020

Just Accepted

is published by the American Chemical Society. 1155 Sixteenth Street N.W., Washington, DC 20036

A Novel Model System for Understanding Anti-Cancer Activity of Hypoxia-Activated Prodrugs

Zhiyuan Sun[1], Haoqi Zhang[1,2], Jin Wu[1], Fangli Gao[1], Congcong Zhang[3], Xueyan Hu[1], Qiqi Liu[1], Yonghua Wei[1,2] Jie Zhuang[1,2]*, Xinglu Huang[1]*

[1]Key Laboratory of Bioactive Materials, Ministry of Education, College of Life Sciences, and State Key Laboratory of Medicinal Chemical Biology, Nankai University, Tianjin 300071, China.

[2]College of Medicine, Nankai University, Tianjin 300071, China.

[3]College of Chemistry and Material Science, Shandong Agricultural University, Taian, P.R.China 271018

*To whom correspondence may be addressed. Email: huangxinglu@nankai.edu.cn or zhuangj@nankai.edu.cn

TOC

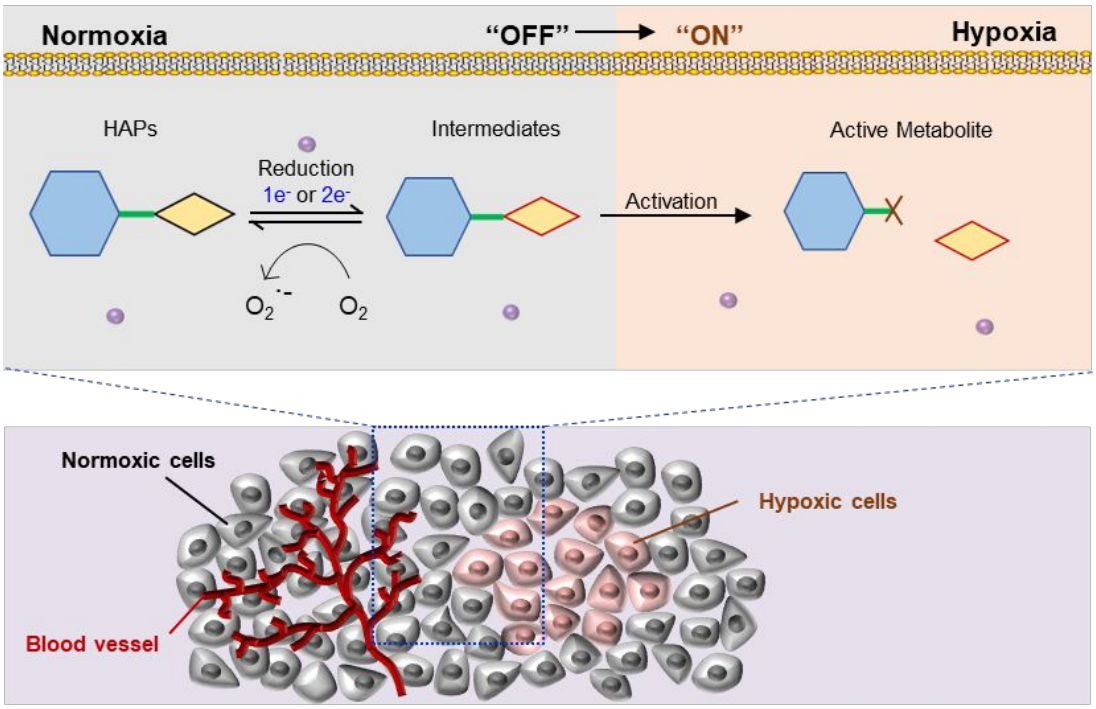
Normoxia
"OFF"
"ON"
Hypoxia
HAPs
Intermediates
Active Metabolite
Reduction
1e- or 2e-
Activation
O2 .-
O2
Normoxic cells
Hypoxic cells
Blood vessel

ABSTRACT

Reports on the comprehensive factors for design considerations of hypoxia-activated prodrugs (HAPs) are rare. We introduced a new model system composed of a series of highly water-soluble HAPs, providing a platform to comprehensively understand the interaction between HAPs and hypoxic biosystems. Specifically, four kinds of new HAPs were designed and synthesized; containing the same biologically active moiety but masked by different bioreductive groups. Our results demonstrated the activity of the prodrugs was strongly dependent on not only molecular structure but also the hypoxic tumor microenvironment. We found the presence of a direct linear relationship between cytotoxicity of the HAPs and the reduction potential of whole molecule/oxygen concentration/reductase expression. Moreover, limited blood vasculature in hypoxic regions was also a critical barrier for effective activation of the HAPs. This study offers a comprehensive insight to understanding the design factors required for HAPs.

Keywords: hypoxia; prodrugs; drug delivery; tumor; mechanism

INTRODUCTION

Hypoxia is a common feature in solid tumors and plays an important role in the occurrence and development of tumors, including but not limited to the promotion of tumor angiogenesis, modulation of tyrosine kinase signal pathways and increase of tumor invasion and metastasis[1-5]. As such, tumor hypoxia has been considered as an extremely valuable target, and there are many reports on detecting tumor hypoxic status and optimizing tumor hypoxic therapy strategies[6, 7]. In particular, taking advantage of the tumor hypoxic characteristics to aid the design of hypoxia-activated prodrugs (HAPs) can specifically functionalize drug molecules within tumor hypoxic regions, while reducing toxicity to normal tissues[8-10]. The mechanism of HAPs is as follows: the prodrug is reduced to form a free radical intermediate in tissues, and can return to the parent prodrugs when in normal tissues, under normoxic conditions. Whereas in hypoxic cells, the intermediate form is cleaved to release the active drug molecules, and this in turn, selectively acts on hypoxic cancer cells[11-13]. Until now, commonly used HAPs mainly include nitrogen oxides (aliphatic and aromatic), anthraquinones, nitro compounds and metal complexes[1, 11, 14]. Among them, nitro-activated prodrugs present good tumor hypoxia specificity, which has greatly promoted the development of the HAPs with nitroimidazoles, such as TH-302[15, 16]. However, TH-302 has failed in clincal trials[17] since it did not achieve primary overall survival endpoints in combination with chemotherapy in two large phase III studies in advanced unresectable or metastatic pancreatic adenocarcinoma (NCT01746979) and in soft tissue sarcoma (NCT01440088). Therefore, we are required to rethink the factors and design considerations of HAPs.

Previous studies have demonstrated that the most important consideration for HAPs design, in principle, is choosing the appropriate bioreductive groups[18, 19]. In other

words, the determinant factor is the propensity of a particular group to undergo bioreduction and the oxygen concentration at which this process occurs. In addition, the factors of biological system also affect the activity of HAPs, such as reductase expression and hypoxic tissue barriers. For example, solubility of HAPs greatly affects the anti-cancer activity, which in essence is due to improved tissue penetration into tumor hypoxic regions that are absent of blood vessel distribution[20-23]. While these factors have been identified individually, it is still necessary to understand which factor(s) play determined roles or whether these factors affect each other. Thus, a comprehensive understanding of the relationship among various factors in HAPs design is necessary, but this has seldomly been reported, owing to the absence of ideal systems.

To address the above requirements, we designed a series of new HAPs that were composed of the same biologically active moiety but each was masked by different bioreductive groups (red R), including nitrobenzofuran, nitrothiazole, nitrothiophene and nitrofuran (Scheme 1). These bioreductive groups were utilized as electron-attracting initiators for increasing electron affinity of the HAPs[24]. The reductases in cells resulted in the occurrence of electron transfer, which in turn reduced the HAPs to form intermediates. The intermediates, in hypoxic tumor tissues, were cleaved to release the cytotoxic moiety for tumor growth inhibition, which was similiar to nitrogen oxides HAPs activity. We explored the effect of various factors on anti-cancer activity of the HAPs, including reduction potential of both whole molecules and bioreductive groups, oxygen concentration and reductase expression. *In vivo* anti-tumor effects and the interaction between the HAPs and hypoxic microenvironment were also investigated.

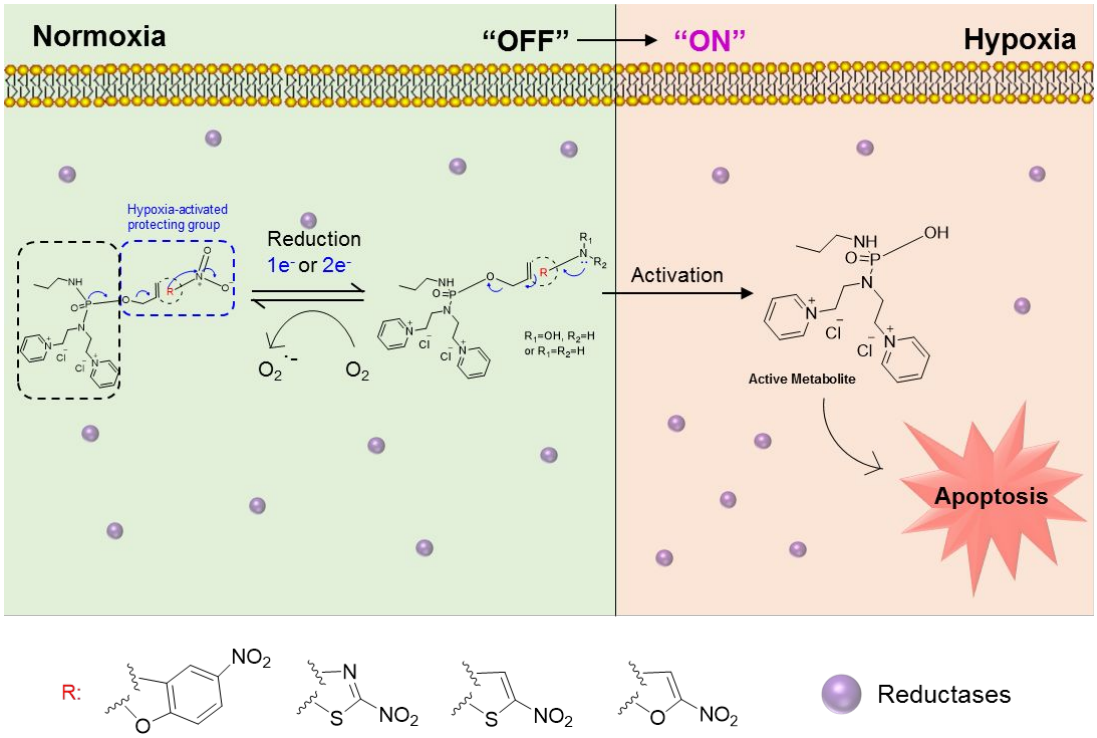

Scheme 1. Schematic illustration of activation of the HAPs in hypoxia. The four kinds of HAPs were designed by containing cytotoxic moiety and different bioreductive groups (R). The bioreductive groups initiated electron transfer under the action of reducctases, to form intermediates. The produced intermediates could return to the parent prodrugs in normoxic cells but be cleaved to release the cytotoxic moiety in hypoxic cancer cells, which in turn selectively induced their apoptosis. The four bioreductive groups included nitrobenzofuran, nitrothiazole, nitrothiophene and nitrofuran (R, from left to right).

EXPERIMENTAL SECTION

General. All solvents were spectroscopic grade and were purified by distillation before use. NMR spectra were recorded by Bruker AVANCE III 400 (400 MHz) spectrometer with deuterium generation reagent and tetramethylsilane as an internal standard. Electrochemical examinations were performed by cyclic voltammetry (CV) in acetonitrile at a scanning rate of 50 mv s^{-1}. Platinum-electrodes (diameter 0.5 mm) served as working electrode and counter electrode. The electrolyte was acetonitrile (5.0 mL) containing 0.5 mmol tetrabutylammonium hexafluorophosphate and 0.2 mmol HAPs.

Prodrug Synthesis. We synthesized four new hypoxia prodrugs (Chinese application patent: 201910650638.2) and the detailed routes were shown in Scheme S1. All

compound structures were characterized by NMR and mass spectra. The detailed synthetic procedures were as follows.

HAPs precursor 2 [2a-2d]

(5-nitrobenzofuran-2-yl) methanol [2a]

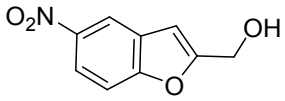

2a

Sodium borohydride (1.2 g, 30 mmol) was added to a solution of tetrahydrofuran: methanol (10:1) containing 1a (1.41 g, 10 mmol). The mixtures reacted for 1 h at ice-bath. After that, the solution was stirred for 1 h and then warmed to the room temperature for 1 h. The suspension was extracted with dichloromethane for organic layer collection, and then washed with NaCl solution and water, respectively. The resulting product was dried over $MgSO_4$, filtrated, and evaporated. The crude product was purified by column chromatography on silica gel using petroleum ether: ethyl acetate (4:1) as eluent to give 2a (1.23 g, 63.5%). ^{1}H NMR (400 MHz, $CDCl_3$) δ (ppm) 4.85 (d, 2H, J = 8.0 Hz, -CH_2), 6.83 (s, 1H, benzofuryl-H), 7.56 (d, 1H, J = 8.0 Hz, benzofuryl-H), 8.24 (d, 1H, J = 8.0 Hz, benzofuryl-H), 8.51 (s, 1H, benzofuryl-H).

(5-nitrothiazole-2-yl) methanol [2b]

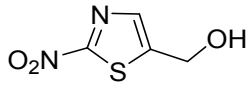

2b

2b was prepared by an analogous method to that used for compound 2a, specifically using 1b instead of 1a. The crude product was purified by column chromatography on silica gel using petroleum ether: ethyl acetate (5:1) as eluent to obtain 2b (1.12 g, 70%). ^{1}H NMR (400 MHz, $CDCl_3$) δ (ppm) 4.42 (d, 2H, J = 8.0 Hz, -CH_2), 8.52 (s, 1H, thiazolyl-H).

(5-nitrothiophene -2-yl) methanol [2c]

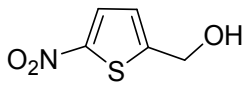

2c

Sodium borohydride (0.6 g, 15 mmol) was added to a solution of methanol containing 5-nitrothiophene-2-carbaldehyde 1c (1.57 g, 10 mmol). The mixtures reacted for 10 min at ice-bath. After that, the solution was stirred for 20 min and then warmed to the room temperature. After 3 h, the suspension was extracted with dichloromethane, and then the organic layer was collected for further washing with NaCl solution and water, respectively. The organic layer was dried over $MgSO_4$, filtrated, and evaporated. The crude product was purified by column chromatography on silica gel using petroleum ether: ethyl acetate (5:1) as eluent to obtain 2c (1.39 g, 88.6%). ^{1}H NMR (400 MHz, $CDCl_3$) δ (ppm) 4.88 (d, 2H, J = 8.0 Hz, -CH_2), 6.94 (d, 1H, J = 8.0 Hz, thienyl-H), 7.82 (d, 1H, J = 8.0 Hz, thienyl-H).

(5-nitrofuran-2-yl) methanol [2d]

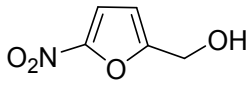

2d

2d was prepared by an analogous method to that used for compound 2c, specifically using 1d instead of 1c. The crude product was purified by column chromatography on silica gel using petroleum ether: ethyl acetate (4:1) as eluent to obtain 2d (0.91 g, 62.9%). ^{1}H NMR (400 MHz, $CDCl_3$) δ (ppm) 5.01 (d, 2H, J = 8.0 Hz, -CH_2), 6.94 (d, 1H, J = 8.0 Hz, furyl-H), 7.54 (d, 1H, J = 8.0 Hz, furyl-H).

HAPs precursor 3 [3a-3d]. A 1.0 M lithium bis(trimethylsilyl)amide in anhydrous THF solution (2.2 mL, 2.2 mmol) was added to raw material 2a-2d (2.0 mmol) in THF at 195 K under an argon atmosphere. Stirring was continued for 0.5 h and bis(2-chloroethyl)phosphoramidic dichloride (0.56 g, 2.2 mmol) was slowly added to the reaction mixture at 195 K and stirred for 2 h at this temperature. After that, propane

diamine in THF was added to the mixture and continued stirring for 1 h at 195 K. Then the reaction was warmed to room temperature and quenched with water. The organic layer was dried over $MgSO_4$, filtrated, and evaporated. The crude product was purified by column chromatography on silica gel using petroleum ether: ethyl acetate (1:1) as eluent to acquire 3a-3d.

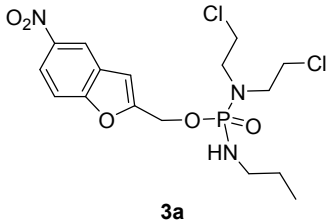

3a

(5-nitrobenzofuran-2-yl)methyl-N,N,N-bis(2-chloroethyl)-1-propan-phosphorodiamidate [3a] (0.39g, 44.6%): ^{1}H NMR (400 MHz, $CDCl_3$) δ (ppm) 0.82-0.86 (m, 3H, -CH_3), 1.37-1.43 (m, 2H, -CH_2), 2.65-2.71 (m, 2H, -CH_2), 3.20-3.33 (m, 4H, -CH_2), 3.62-3.68 (m, 4H, -CH_2), 5.07 (d, 2H, J = 8.0 Hz, -CH_2), 7.21 (s, 1H, benzofuryl-H), 7.84 (d, 1H, J = 8.0 Hz, benzofuryl-H), 8.24 (d, 1H, J = 12.0 Hz, benzofuryl-H), 8.66 (s, 1H, benzofuryl-H).

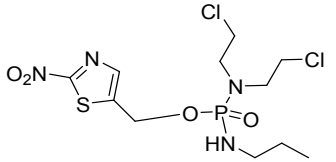

3b

(5-nitrothiazole-2-yl)methyl-N,N,N-bis(2-chloroethyl)-1-propan-phosphorodiamidate [3b] (0.21g, 26.1%): ^{1}H NMR (400 MHz, $CDCl_3$) δ (ppm) 0.92-0.95 (m, 3H, -CH_3), 1.38-1.41 (m, 2H, -CH_2), 1.56-1.62 (m, 2H, -CH_2), 3.51-3.64 (m, 4H, -CH_2), 4.37-4.42 (m, 4H, -CH_2), 5.14 (d, 2H, J = 8.0 Hz, -CH_2), 8.52 (s, 1H, thiazolyl-H).

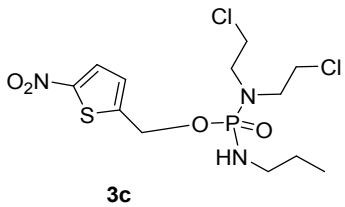

3c

(5-nitrothiophene-2-yl)methyl-N,N,N-bis(2-chloroethyl)-1-propan-phosphorodiamidate [3c] (0.27g, 33.5%): ^{1}H NMR (400 MHz, $CDCl_3$) δ (ppm) 0.91-0.95 (m, 3H, -CH_3), 1.51-1.55 (m, 2H, -CH_2), 2.87-2.90 (m, 2H, -CH_2), 3.42-3.47 (m, 4H, -CH_2), 3.63-3.66 (m, 4H, -CH_2), 5.16 (d, 2H, J = 8.0 Hz, -CH_2), 7.02 (d, 1H, J = 4.0 Hz, thienyl-H), 7.82 (d, 1H, J = 4.0 Hz, thienyl-H).

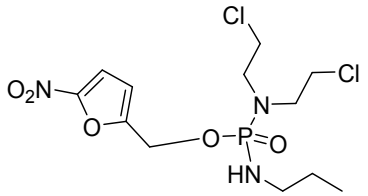

3d

(5-nitrofuran-2-yl)methyl-N,N,N-bis(2-chloroethyl)-1-propan-phosphorodiamidate [3d] (0.33g, 42.1%): ^{1}H NMR (400 MHz, $CDCl_3$) δ (ppm) 0.91-0.94 (m, 3H, -CH_3), 1.50-1.56 (m, 2H, -CH_2), 2.86-2.92 (m, 4H, -CH_2), 3.39-3.45 (m, 2H, -CH_2), 3.62-3.67 (m, 4H, -CH_2), 5.03 (d, 2H, J = 8.0 Hz, -CH_2), 6.65 (d, 1H, J = 4.0 Hz, furyl-H), 7.27 (d, 1H, J = 4.0 Hz, furyl-H).

Hypoxia-activated prodrugs [H1-H4]. 3a-3d (1 mmol) were dissolved in pyridine (10 ml) under stirring. The reaction mixture was reacted at 100°C for 24 h under nitrogen atmosphere. The crude product was purified by oil washed many times through dichloromethane and ethyl acetate. The collected precipitation was dissolved in ultrapure water for freeze-drying by lyophilizer to obtain H1-H4.

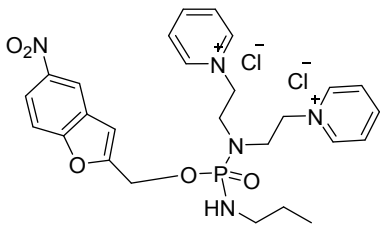

H1

1,1'-(((((5-nitrobenzofuran-2-yl)methoxy)(propylamino)phosphoryl)azanediyl) bis(ethane-2,1-diyl))bis(pyridin-1-ium) chloride [H1] (0.25g, 42.1%): ^{1}H NMR (400

MHz, D_2O) δ (ppm) 1.00-1.06 (m, 3H, -CH_3), 1.68-1.73 (m, 2H, -CH_2), 2.89-2.93 (m, 2H, -CH_2), 3.21-3.24 (m, 4H, -CH_2), 4.69-4.72 (m, 4H, -CH_2), 5.04 (d, 2H, J = 8.0 Hz, -CH_2), 7.47 (s, 1H, benzofuryl-H), 7.72 (d, 1H, J = 8.0 Hz, benzofuryl-H), 8.02 (d, 1H, J = 8.0 Hz, benzofuryl-H), 8.08-8.24 (m, 4H, pyridyl-H), 8.59-8.71 (m, 2H, pyridyl-H), 8.68 (s, 1H, benzofuryl-H), 9.10-9.12 (m, 2H, pyridyl-H), 9.21-9.22 (m, 2H, pyridyl-H). MS (ESI):m/z-2Cl Calcd for $C_{26}H_{32}Cl_2N_5O_5P$ 595.1518; found 524.2304.

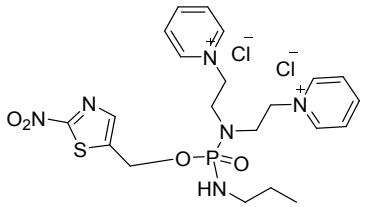

H2

1,1'-(((((2-nitrothiazol-5-yl)methoxy)(propylamino)phosphoryl)azanediyl)bis(ethane-2,1-diyl))bis(pyridin-1-ium) chloride [H2] (0.20g, 35.6%): ^{1}H NMR (400 MHz, D_2O) δ (ppm) 0.88-0.90 (m, 3H, -CH_3), 1.24-1.28 (m, 2H, -CH_2), 1.38-1.40 (m, 2H, -CH_2), 4.10-4.15 (m, 4H, -CH_2), 4.40-4.45 (m, 4H, -CH_2), 4.97 (d, 2H, J = 8.0 Hz, -CH_2), 8.03-8.19 (m, 4H, pyridyl-H), 8.51 (s, 1H, thiazolyl-H), 8.55-8.65 (m, 2H, pyridyl-H), 8.85-8.86 (m, 2H, pyridyl-H), 9.12-9.13 (m, 2H, pyridyl-H). MS (ESI):m/z-2Cl Calcd for $C_{21}H_{29}Cl_2N_6O_4PS$ 562.1086; found 491.2032.

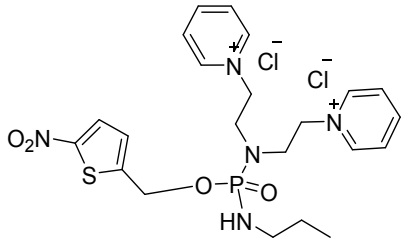

H3

1,1'-(((((5-nitrothiophen-2-yl)methoxy)(propylamino)phosphoryl)azanediyl)bis(ethane-2,1-diyl))bis(pyridin-1-ium) chloride [H3] (0.25g, 43.8%): ^{1}H NMR (400 MHz, D_2O) δ (ppm) 1.02-1.06 (m, 3H, -CH_3), 1.70-1.72 (m, 2H, -CH_2), 2.89-2.93 (m, 2H, -CH_2), 3.15-3.26 (m, 4H, -CH_2), 4.72-4.75 (m, 4H, -CH_2), 5.17 (d, 2H, J = 8.0 Hz, -CH_2), 7.91 (d, 1H, J = 8.0 Hz, thienyl-

H), 8.03-8.10 (m, 4H, pyridyl-H), 8.24 (m, 1H, thienyl-H), 8.56-8.60 (m, 2H, pyridyl-H), 8.85-8.86 (m, 2H, pyridyl-H), 8.92-8.93 (m, 2H, pyridyl-H). MS (ESI):m/z-2Cl Calcd for $C_{22}H_{30}Cl_2N_5O_4PS$ 561.1133; found 490.1246.

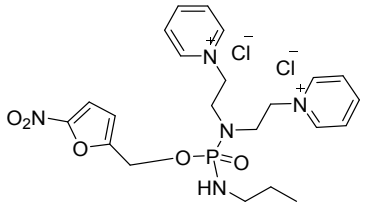

H4

1,1'-(((((5-nitrofuran-2-yl)methoxy)(propylamino)phosphoryl)azanediyl)bis(ethane-2,1-diyl))bis(pyridin-1-ium) chloride [H4] (0.20g, 37.2%): ^{1}H NMR (400 MHz, D_2O) δ (ppm) 1.02-1.06 (m, 3H, -CH_3), 1.68-1.73 (m, 2H, -CH_2), 2.89-2.93 (m, 4H, -CH_2), 3.32-3.34 (m, 2H, -CH_2), 3.67-3.68 (m, 4H, -CH_2), 5.06 (d, 2H, J = 8.0 Hz, -CH_2), 6.82 (d, 1H, J = 4.0 Hz, furyl-H), 7.45 (d, 1H, J = 4.0 Hz, furyl-H), 8.08-8.17 (m, 4H, pyridyl-H), 8.60-8.66 (m, 2H, pyridyl-H), 8.90-8.92 (m, 2H, pyridyl-H), 9.00-9.03 (m, 2H, pyridyl-H). MS (ESI):m/z-2Cl Calcd for $C_{22}H_{30}Cl_2N_5O_5P$ 545.1362; found 474.1878.

Human and Mouse Cell lines. 4T1 mouse breast cancer cells were cultured in RPMI 1640 supplemented with 10% fetal bovine serum (FBS, BI) and 1% penicillin/streptomycin (PS, HyClone). HepG2 human liver carcinoma cell, U87 human brain glioblastoma cells, HT1080 human fibrosarcoma cells, PC3 human prostate cancer cells, 3LL mouse lung cancer cells and B16 mouse melanoma cells were cultured in DMEM high glucose (HyClone) supplemented with 10% FBS and 1% PS. For normoxic and hypoxic cell culture, cells were incubated in a humidified incubator (37 ^{o}C, 5% CO_2) with normoxic (21% O_2) or hypoxic (10%, 5%, 2% or 0.5% O_2) conditions, respectively.

Cell colony formation assay. HepG2 and 3LL cells were digested by 0.25% trypsin/0.02% EDTA solution to make a single cell suspension. Then, the cells were seeded into six-well culture plates at the indicated densities (500, 1000, and 2000 cells

per well), treated with H3 or H4 under various oxygen concentrations for 7 days, fixed with 4% PFA and stained with 1.25% crystal violet solution for quantification[25, 26].

Cytotoxicity in monolayer cell. Cytotoxicity was measured using standard MTT assay. Briefly, 4×10^3 cells were seeded into 96-well plates, and then were treated with the prodrugs H1-H4 (0, 20, 50, 100 and 200 μM) at normoxic or hypoxic conditions, respectively. After 24 h incubation, 10 μL MTT was added to each well and DMSO was added to the media 4 h later. Finally, OD_{570} was measured by Thermo Scientific Microplate Reader. The cell viability was calculated as OD_{570} mean value in experimental group/OD_{570} mean value in control group × 100%.

Apoptosis assay. HepG2 cells were treated with 200 μM H1-H4 under hypoxic condition (0.5% O_2) for 24 h, and then stained with Annexin V-FITC and propidium iodide (PI) according to manufacture protocol (Beyotime Biotechnology, China). Briefly, 1×10^5 cells were washed with cold PBS and suspended with 100 μl binding buffer. 5 μl of Annexin V-FITC was added to the cells for 10 min. After incubation, 5 μl PI was added for 5 min. Finally, the cells were analyzed by flow cytometry (BD FACSCalibur, USA) [27].

Cell cycle analysis. HepG2 cells were treated with 200 μM H1-H4 under hypoxic condition (0.5% O_2) for 24 h, respectively and then stained with PI according to manufacture protocol (Beyotime Biotechnology, China). Briefly, the cells were harvested and washed with cold PBS, fixed in ice-cold 75% ethanol overnight at 4 °C. The fixed cells were collected by centrifugation, resuspended in 500 μl stain buffer and incubated with 25 μl PI and 10 μl RNase A at 37 °C for 30 min in dark. Finally, the cells were analyzed by flow cytometry (BD FACSCalibur, USA).

HAPs reduction assay *in vitro*. 100 mM HAPs were placed into PB buffer (pH 7.4), followed by 100 mM NADPH, and incubated with P450 oxidoreductase (POR) (Life

Technologies) in a humidified incubator (37 °C, 5% CO_2) with hypoxic (0.5% O_2) conditions. The FL spectra of HAPs was monitored by Bio-Rad Enzyme Marker. After 24 h, the crude mixtures were purified by column chromatography on silica gel plate.

Real-Time PCR assays. Total RNA was isolated from cells using TRIzol (Solarbio, China) according to the manufacturer protocol. Reverse transcription reaction to synthesize complementary DNAs (cDNAs) was performed using 2 μg of total RNA and 4 μl 5X ALL-In-One RT Master Mix (Abm, China) in an RNase-free environment. Real-Time PCR was performed with the QuantStudio™ 3 Real-Time PCR System (Appled Biosystems). The results were normalized by measuring average cycle threshold (Ct) ratios between POR and the housekeeping gene EIF3F (TIF). PCR sequences are provided below.

Human POR

F 5'- TCAATGCCATGGGCAAGTA-3'

R 5'- ATGAAGTCCTCCTCCAAGTTC-3'

Human TIF

F 5'- GACACAAGTCTCCAGAACGGC-3′

R 5'- TGGTCTCAAAGTCATCGGGAA-3′

Mouse POR

F 5'- TCCTGACCTACTGGTTCATCT-3′

R 5'- CACGAAGCTGCTCTCTTTGA-3′

Mouse TIF

F 5'- CTGAGGATGTGCTGTCTGGGAA-3′

R 5'- CCTTTGCCTCCACTTCGGTC-3′

Xenograft model. Male BALB/c-Nude mice (5–6 weeks old) and female C57 mice (6-8 weeks old) were purchased from SPF (Beijing) Biotechnology Co. Ltd. All animals

and *in vivo* experiments were in compliance with governmental and international animal guidelines. 2×10^6 HepG2, 2×10^6 U87 or 5×10^5 3LL cells were subcutaneously injected into right shoulder of the mice, respectively, and then assigned randomly to different groups (5-6 mice per group). Treatments with H3 or H4 (40 mg/kg) were initiated when tumors reached a diameter ~5 to 8 mm. The mice were treated intravenously every day (3LL xenografted tumor) or intraperitoneal injection every other day (HepG2 and U87 xenografted tumor) for 5 doses total. The tumor volume was measured every day, and was calculated by the formula: $(\text{width})^2 \times (\text{length})/2$. Body weight of the mice was also monitored.

Hypoxia and blood vessel staining. After HAPs treatment, the pimonidazole HCl (60 mg/kg) was given to mice 1.5 h prior to euthanization. The tumor tissues were immunostained with Hypoxyprobe following the manufacturer's procedures (Hypoxyprobe, Inc). Briefly, the hypoxic regions of the tumor were stained using FITC-conjugated anti-pimonidazole antibody. To co-stain with blood vessels, the tissues were simultaneously incubated with PE-conjugated anti-CD31 antibody (Biolegend). The images were acquired by confocal laser-scanning microscope (Zeiss LSM 710) and analyzed via Image J.

TUNEL staining. The tumor frozen sections were prepared after HAPs treatment and then TUNEL staining was performed according to manufacturer instruction of one-step fluorescent TUNEL Apoptosis Assay Kit (Beyotime Biotechnology, China). Briefly, the frozen sections were fixed with 4% PFA for 30 min, permeabilized by 0.2% Triton X-100, and stained with TUNEL staining solution for 1 h. The images were captured using a confocal laser-scanning microscope (Zeiss LSM 710) and quantified by ImageJ. The proportion of TUNEL signal in the tumor hypoxic or normoxic tissues was

evaluated by following the formula A_T/A_H (or A_N): A_T represents the area of TUNEL regions; A_H is the area of hypoxic tissues; A_N is the area of normoxic tissues.

Statistical analysis. The Student's unpaired t-test was used for statistical analysis between two groups of independent data. If multiple comparisons were involved, one-way or two-way ANOVA was used as needed. Differences were considered statistically significant at $P < 0.05$. Results were shown as the mean ± SEM.

RESULTS AND DISCUSSION

Design and synthesis of prodrugs

The designed prodrugs mainly contained two components, including the biologically active moiety and bioreductive groups. As a model effector molecule, phosphoramide mustard was chosen based on the below considerations: 1) it is a biologically active metabolite of cyclophosphamide, a chemotherapeutic agent commonly used to treat lymphomas, breast cancers, certain brain cancers, and autoimmune diseases[28-30]; 2) it easily reacts with the four bioreductive groups. Given its critical role in hypoxic tumor penetration, water-solubility of HAPs was further improved by introduction of pyridinium. The designed bioreductive groups possessed different reduction potential ranking: nitrobenzofuran (2a) < nitrothiazole (2b) < nitrothiophene (2c) < nitrofuran (2d) (Fig. 1). Following conjugation with phosphoramide mustard cytotoxic components and pyridinium, the reduction potential of the obtained HAPs (H) corresponding to the bioreductive groups was -1.45 V (H1), -1.39 V (H2), -1.32 V (H3) and -1.56 V (H4) via cyclic voltammetry characterization, respectively. Due to the prodrugs embedding an identical cytotoxic component but having varied bioreductive groups, this provided a well-designed and new model system, as a platform to understand not only the relevance among molecular structures, the

reduction potential of whole HAPs molecules and oxygen concentration but also the interaction between the HAPs and biological systems.

Four kinds of novel hypoxia-responsive prodrugs were synthesized by multiple step reactions of different nitro group-based precursor molecules with phosphoramide mustard. In a typical reaction, nitro-based aromatic aldehydes (i.e. nitrobenzofuran, nitrothiazole, nitrothiophene and nitrofuran) were reduced by sodium borohydride in methanol or tetrahydrofuran[31]. The resulting molecules were subsequently conjugated with phosphoramide mustard to obtain major components of the HAPs. To improve the water-solubility of HAPs [32, 33], pyridine cationization reaction was further performed. The detailed reaction routes were shown in Scheme S1. The successful synthesis of four prodrugs was confirmed by NMR characterization. These HAPs displayed high solubility, with >100 mg/ml in water solution.

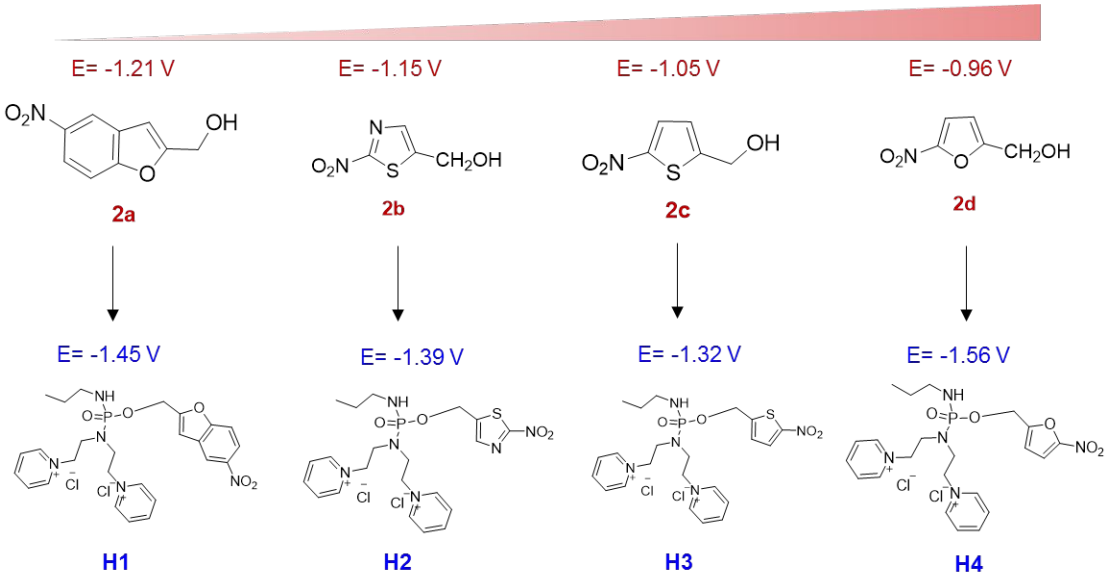

Figure 1. Molecular structures and reduction potential of different bioreductive groups (upper) and the corresponding HAPs (bottom).

Cytotoxicity of different HAPs under various O_2 concentrations

We further explored whether the four prodrugs, H1-H4, could be activated under hypoxia. As such, different cancer cells such as HepG2 and 3LL cells were cultured at

0.5% O_2 for evaluation of the activity of the prodrugs, and this was followed by assessment by standard cell activity assays. All four of the prodrugs showed a concentration-dependent inhibition effect on HepG2 and 3LL cells, especially H4 (Fig. 2A). The inhibition ability of H4 on HepG2 was 2.1-, 4.4- and 6.9-fold higher at the concentration of 200 μM, compared to that of H1, H2 and H3, respectively, which was comparable with 3LL cells. Importantly, we found an excellent linear relationship between the reduction potential of whole HAPs molecules and cell viability for both cancer cells (Fig. 2B), and this was irrelevant to the reduction potential of bioreductive groups (Fig. S1). Since the reduction potential of whole prodrug molecules was ranked as: H4 < H1 < H2 < H3, the lower reduction potential of whole prodrug molecules presented a higher cytotoxicity, which was not cell type dependent. Next, H4 was selected to evaluate whether the cytotoxicity of the prodrugs was oxygen-dependent. Both HepG2 and 3LL cells were cultured at different O_2 concentration (i.e. 21%, 10%, 5%, 2% and 0.5%), and the results showed that the cytotoxicity of H4 was increased along with the reduction of O_2 concentration (Fig. 2C). A linear relationship between O_2 concentration and cell viability was also established, which revealed that the activation of the prodrugs was strongly dependent on hypoxic condition (Fig. 2D). The results were further confirmed by various other cancer cell types, such as U87, HT1080, PC3, 4T1 and B16 (Fig. S2). Based on the above results, the reduction potential of whole HAPs molecules and O_2 concentration determined the activity of the prodrugs. Thus, we further explored the effect of these two aspects on the colony formation capacity of HepG2 cells in response to H4 treatment. The colony formation rate after H4 treatment was about 2-fold reduction at hypoxic condition (0.5% O_2) compared to the untreated groups, while no significant changes of colony formation were observed for H3 treatment under either hypoxic or normoxic conditions (Fig. 2E and F). More

strikingly, the colony formation capacity of H4 treated 3LL cells was decreased by approximately 8-fold under hypoxia, compared to untreated 3LL cells (Fig. S3).

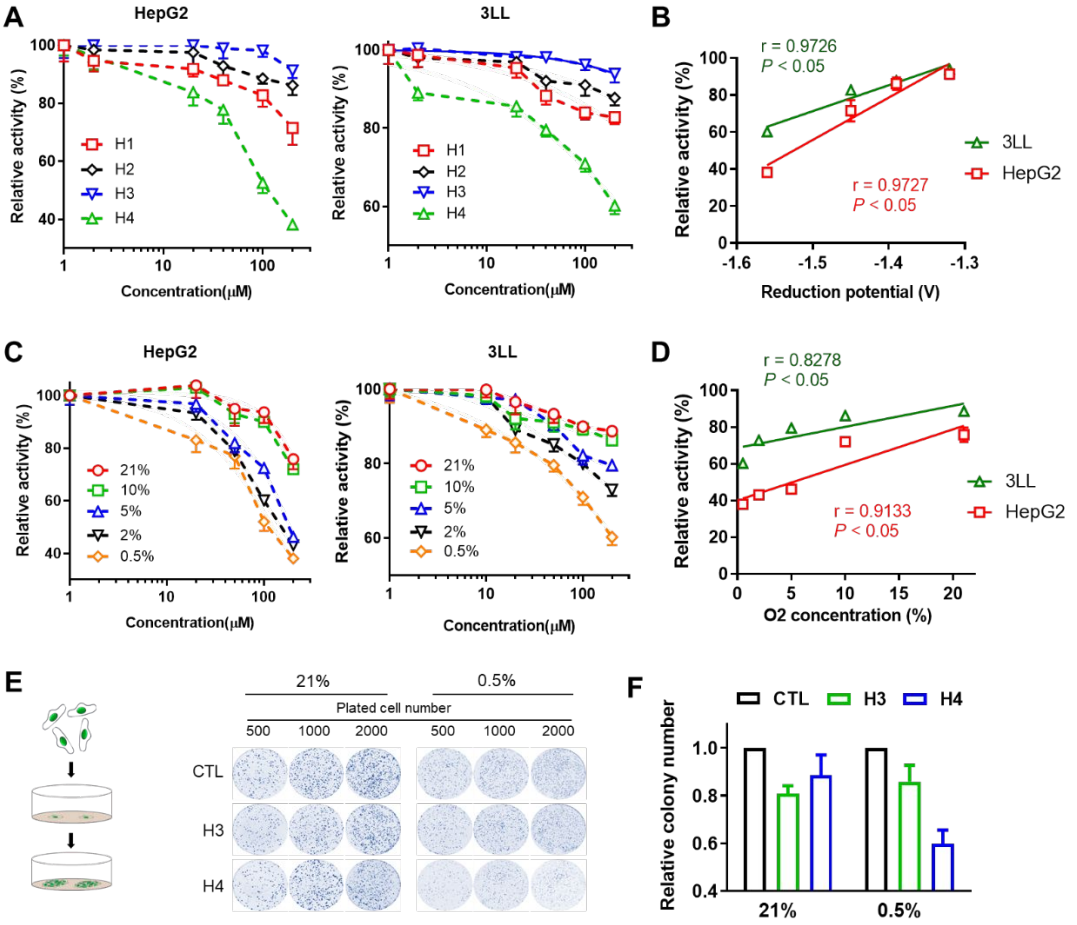

Figure 2. Effect of different HAPs on cancer cells under various O_2 concentrations. (A) Inhibition rate of HepG2 and 3LL cells following treatment with H1-H4 under hypoxia (0.5%) for 24 h, respectively. (B) The linear relationship between cell viabiltiy at 200 μM HAPs and the reduction potential of whole HAPs molecules. (C) Cytotoxicity of H4 for HepG2 and 3LL cells at different O_2 concentrations (i.e. 21%, 10%, 5%, 2% and 0.5%) after 24 h treatment. (D) The linear relationship between cell viability at 200 μM HAPs and O_2 concentration. (E) Representative images and (F) quantification analysis of the colony formation capacity of HepG2 cells treated with H4 under normoxic (21%) and hypoxic (0.5%) conditions for 7 days.

HAPs reduction assay *in vitro*

As shown above in Fig. S2, the cytotoxicity of H4 was obviously varied in different cancer cell types, demonstrating that the activation of H4 under hypoxia was cell type-dependent. It has been identified that the expression level of POR in cancer cells is responsible for the activation of hypoxia-activated prodrugs (HAPs) [34, 35]. We thus

explored whether the cleavage of H4 was POR dependent by incubation H4 with purified POR, together with NADPH as co-substrate for 2 h under hypoxia. The fluorescent signal of H4 showed a 21.5% reduction by comparison before and after POR treatment (Fig. S4). Furthermore, the resulting compound after reaction was purified by column chromatography on silica gel and characterized with NMR, showing a clear peak of nitrofuran following the cleavage of ester linkage of H4 (Fig. 3A). To demonstrate the effect of POR expression on H4 cytotoxicity, we next checked the cytotoxicity of H4 as well as POR expression in various human and mouse cancer cells, including HepG2, U87, PC3, HT1080, 3LL, 4T1 and B16. We found both cytotoxicity (Fig. 3B) and POR expression (Fig. 3C) were cell type-dependent. Interestingly, the cytotoxicity of H4 on different cancer cells was association with POR expression, a correlation that was statistically significant in a pooled analysis of seven different cell lines ($P < 0.05$) (Fig. 3D).

Anti-cancer mechanism

We next sought to understand the detailed molecular mechanism of the HAPs in inhibiting cancer cell growth. HepG2 cells treated with H1-H4 under hypoxia were stained with Annexin V and PI for apoptosis analysis, and the results showed a notable increase of the percentage of apoptotic cells, with ~2.1-fold elevation after H4 treatment compared to untreated cells (Fig. 4A and B). In addition, cell cycle progression of HepG2 treated with H1-H4 was further evaluated by flow cytometry analysis. As shown in Fig. 4C and D, the changes of cell cycle progression occurred after treatment with the prodrugs, especially for H4. After H4 treatment, compared to untreated cells, cells of G0/G1 phase increased from 18.6% to 27.4%, whereas cells in G2/M decreased ~2-fold. Taken together, these data suggest that the prodrug H4 inhibited cancer cell growth

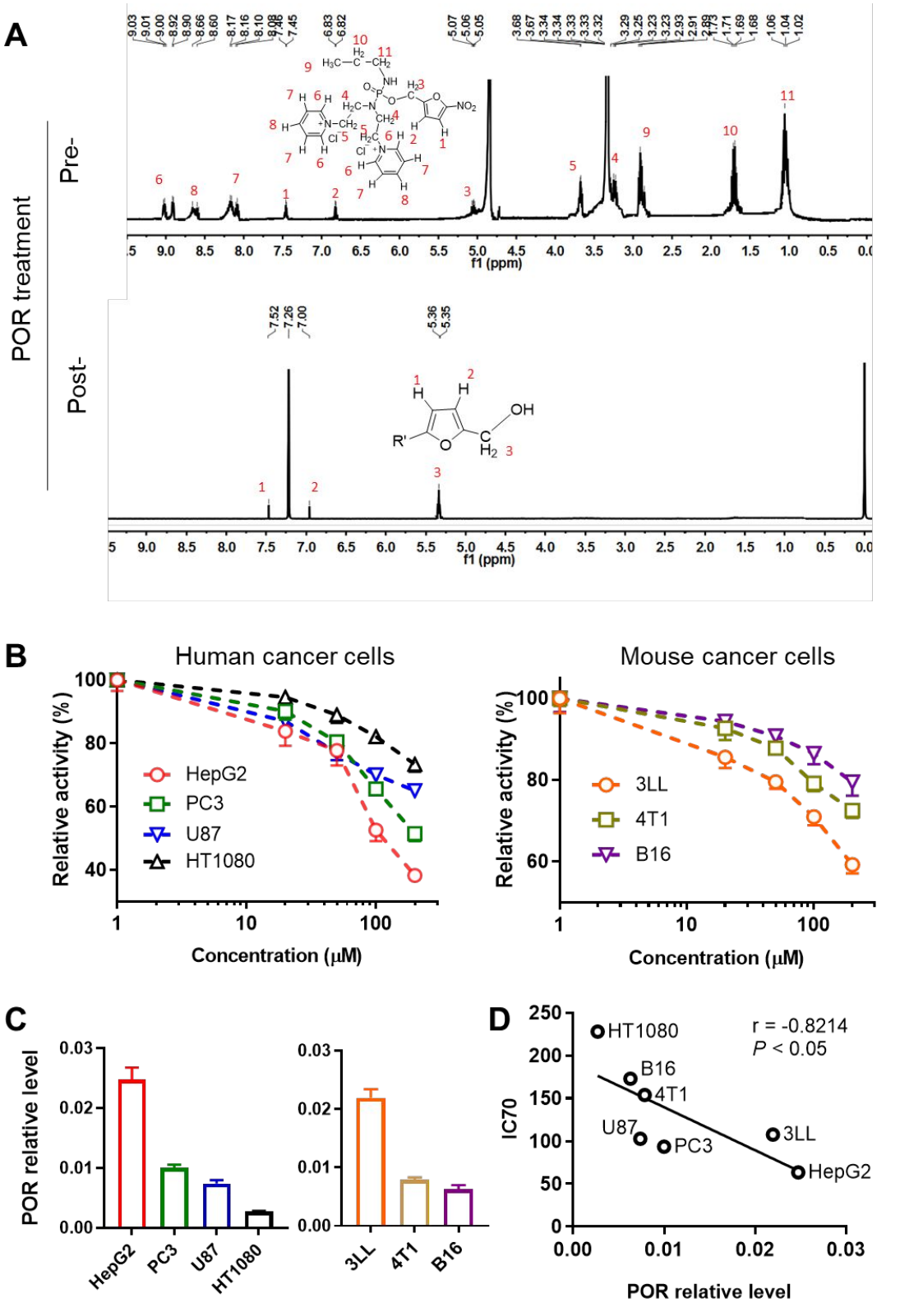

Figure 3. Effect of reductase on H4 activation under hypoxic condition. (A) ^{1}H NMR characterization of H4 and the released bioreductive groups after treated with POR under 0.5% O_2. (B) Inhibition effect of H4 on various human (left) and mouse (right) cancer cells under 0.5% O_2. (C) RT-PCR analysis of POR expression level in various human (left) and mouse (right) cancer cells under 0.5% O_2. (D) The linear relationship between IC_{70} of H4 and POR expression level.

in hypoxic conditions, and this was mainly due to increased cell apoptosis and cell cycle arrest.

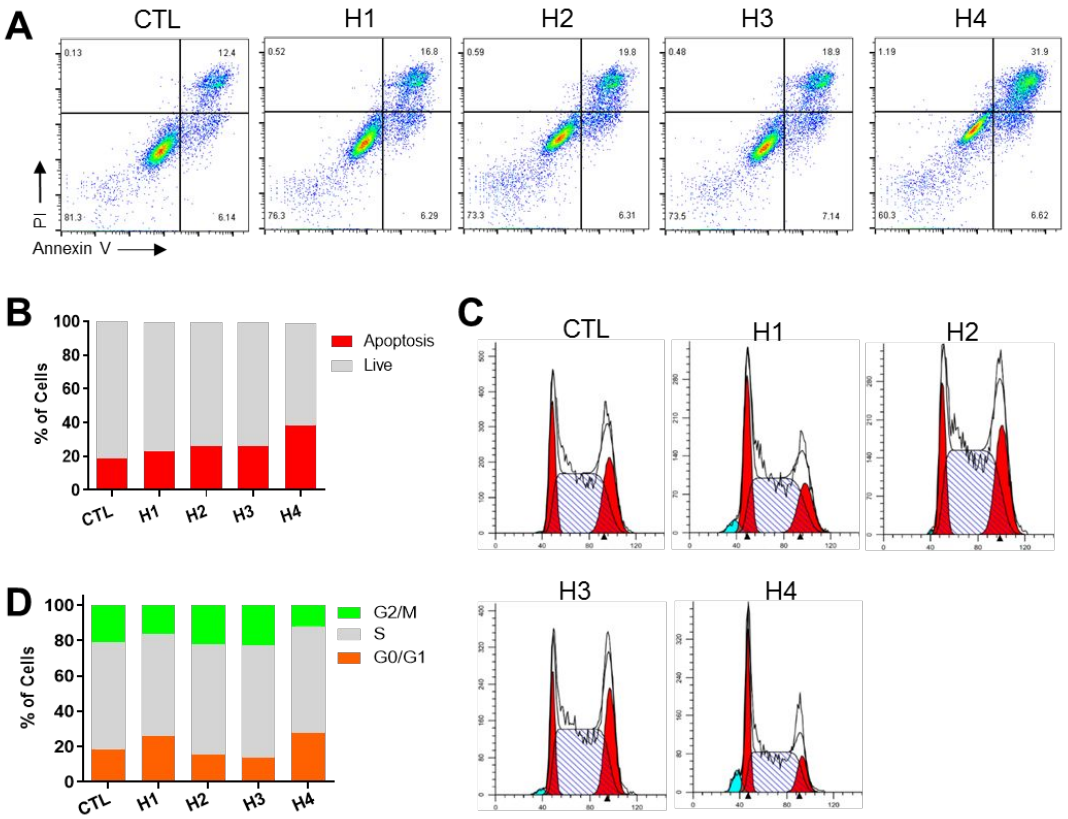

Figure 4. Effect of H1-H4 on HepG2 cell apoptosis and cell cycle. HepG2 cells were treated with H1-H4 under hypoxic condition for 24 h, respectively. (A, B) FACS analysis of untreated control (CTL) and H1-H4 treated cells stained with Annexin V and PI. The relative fraction of live and apoptotic cells was quantified. (C, D) FACS analysis of CTL and H1-H4 treated cells stained with PI. The relative fraction of cells in the different cell-cycle stages (G0/G1, S, G2/M) was quantified.

In vivo anti-cancer effect and activation mechanism of the HAPs

Next, we studied the effect of the prodrugs on *in vivo* tumor growth in various mice models xenografted with HepG2, U87 and 3LL cells. Prior to exploring anti-tumor efficacy of the prodrugs, the occurrence of hypoxia was checked in these three tumor models. The hypoxic areas, blood vessels and cell nuclei of the tumor tissues were stained with anti-pimonidazole antibody (green), anti-CD31 antibody (red) and DAPI (blue), respectively. We found abundant hypoxic regions within tumor, but limited blood vessel distribution was observed in hypoxic regions. The vessel density in

hypoxic area was less than one-third of that in normoxic tumor regions of the same tumor among all three tumor models (Fig. 5A-C), which was consistent with previous reports[1, 36-39]. In other words, direct delivery of the prodrugs into hypoxic regions was really difficult due to the inaccessibility of hypoxic area by systemic administration of therapeutic agents. We then evaluated whether systemically administered prodrugs delayed tumor growth. The mice bearing HepG2, U87 or 3LL were randomly divided into three groups, respectively, and were injected with PBS, H3 (prodrug control) and H4. As shown in Fig. 5D-F, tumor growth was significantly inhibited after H4 treatment for all three tumor models. In contrast, the tumor volume showed no statistical changes in H3 treated groups. Additionally, in all groups of the three tumor models, no significant changes in the body weight of mice were observed, as shown in Fig. S5; suggesting that both H3 and H4 had no apparent systemic toxicity.

The potential *in vivo* anti-cancer mechanism of the prodrugs was further explored. The tumors from HepG2 groups were dissociated to single cell suspension by trypsinization, and then the cells were stained with Annexin V-FITC and PI. As shown in Fig. 6A, a 2.5- and 1.4-fold increase of apoptotic percentage in H4 treated tumor was observed by comparing to that of untreated and H3 treated tumors, respectively. Subsequently, the distribution of apoptotic cells in tumor tissue was analyzed via TUNEL staining for cell apoptosis along with anti-pimonidazole immunostaining for hypoxia. The representative images, shown in Fig. 6B, displayed the substantial increase of cell apoptosis in H4-treated tumor tissues compared to untreated and H3 treated tissues. Quantification analysis of the percentage of positive apoptotic cells in untreated, H3 and H4 tissues accounted for 18.4±0.8, 19.3±1.4 and 28.4±1.3 of total cancer cells, respectively (Fig. 6C). Furthermore, H4-treated tumor tissues presented that cell apoptosis in hypoxic areas was ~15.6-fold higher than nomoxic areas (Fig. 6D)

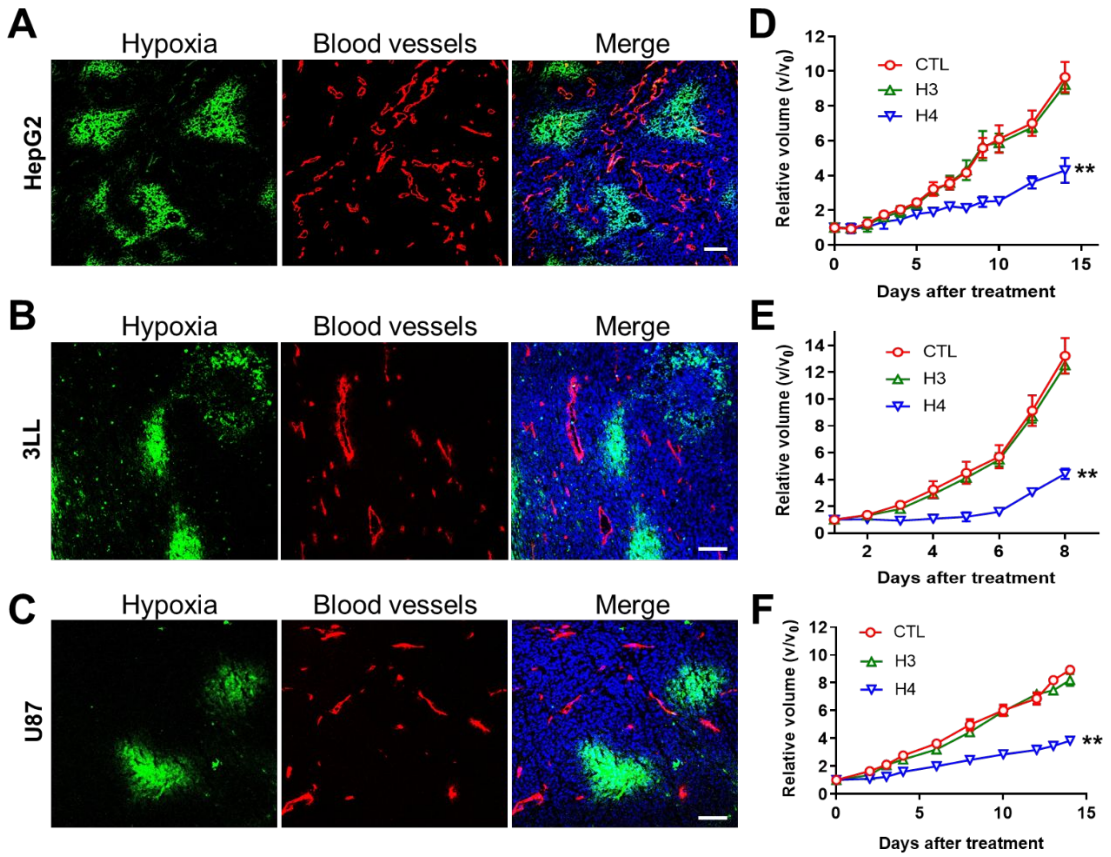

Figure 5. *In vivo* anti-cancer effect of H4 treatment. Representative confocal images of distribution of hypoxia (green) and blood vessels (red) in various xenograft tumor tissues, including (A) HepG2, (B) 3LL and (C) U87. Blue color represents cell nuclei. Scale bar = 100 μm. Tumor growth curve of (D) HepG2, (E) 3LL and (F) U87 untreated or treated with H3 and H4, respectively. n = 6/group. **P<0.01.

and the signal intensity of positive apoptotic cells in tumor tissues was highly concomitant with that of hypoxic status (Fig. 6E), revealing that the occurrence of cell apoptosis mainly localized in hypoxic areas. As shown in Fig. 6A, hypoxic regions of tumors lacked blood vessels and, thus, were not readily accessible by systemically administered therapeutic agents. Thus, the results also implied that our designed H4 prodrugs directly induced cell apoptosis following their penetration into hypoxic tissues, most likely due to their high water-solubility[20, 22, 40]. Given the main action of HAPs on hypoxic cancer cells, and thus, developing hypoxic cell-targeting strategy for HAPs

accumulation into hypoxic cancer cells should be an unneglectable factor for anti-cancer HAPs design.

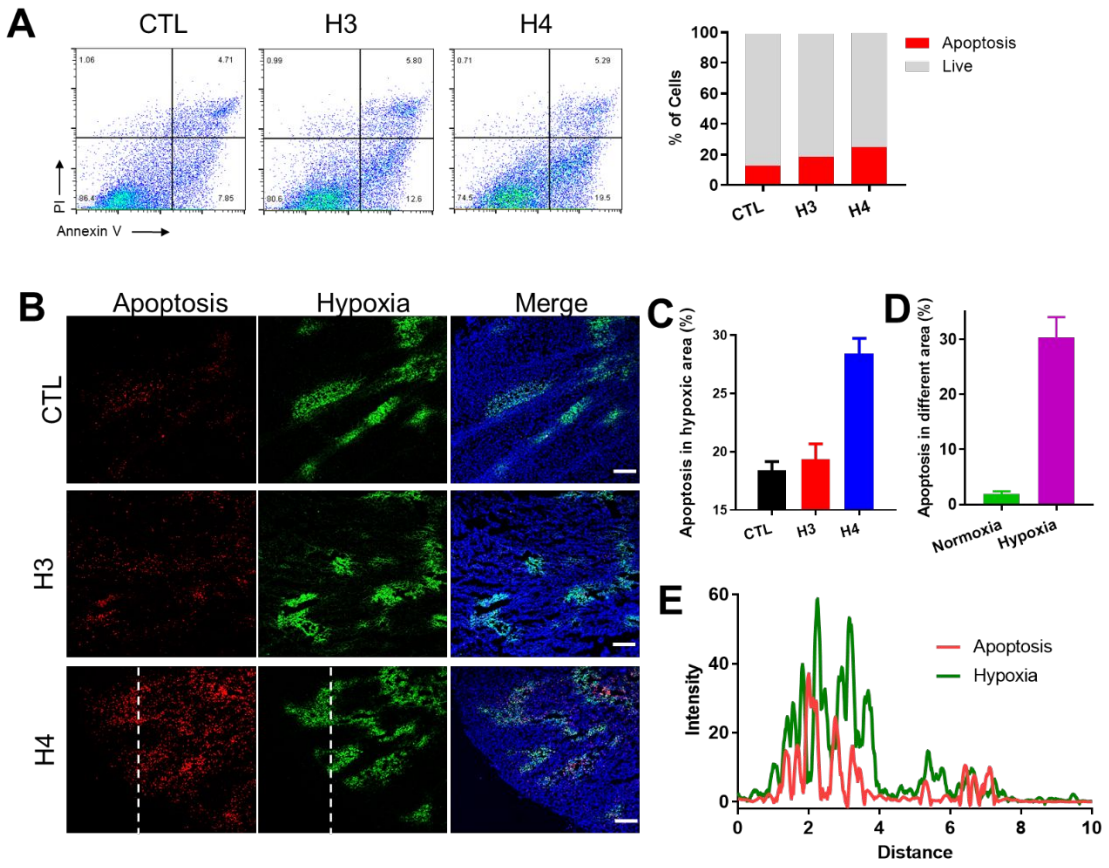

Figure 6. *In vivo* anti-cancer and activation mechanism of HAPs. (A) Flow cytometry and quantification analysis of HepG2 tumor apoptosis by Annexin V and PI staining. (B) Representative images of hypoxia (green) and TUNEL (red) staining of HepG2 tumor tissues following H3 and H4 treatment, respectively. Scale bar = 200 μm. (C) Quantification analysis of apoptosis signal (TUNEL staining) within HepG2 tumor untreated or treated with H3 and H4, respectively. (D) Quantification analysis of apoptosis signal intensity in hypoxic and normoxic tumor tissues following H4 treatment. (E) A co-localization analysis of the distribution of hypoxia and apoptosis in H4 treated tumor tissue based on the plot profile of white cross line from (B).

In conclusion, our designed a series of novel HAPs provided a basis for comprehensive understanding the interaction between hypoxia-targeted prodrugs and hypoxic tumor tissue. By evaluation of the interaction between four HAPs and various cancer cells/tissues, we demonstrated that both molecular structure and hypoxic biological system play critical role in anti-cancer activity of the prodrugs designed. For HAPs molecules design, our results revealed that the larger redox propensity of full HAPs

molecules had the higher anti-cancer property via the release of effector molecules under hypoxia, while the anti-cancer activity was not dependent on the reduction potential of bioreductive activated groups. However, addition of the bioreductive moiety as electron-attracting groups was the prerequisite for increasing electron affinity of HAPs. Thus, both redox properties of full molecules and activated bioreductive groups are necessary design considerations. In biological systems, the linear relationship of reductase enzyme expression or oxygen status with cytotoxicity of the HAPs revealed that tumor heterogeneity was also essential for anti-cancer efficacy of the prodrugs. Remarkably, hypoxic cell-targeting of drug molecules is still a challenging factor, due to limited blood vessels in tumor hypoxic regions. Our designed prodrugs, with high water solubility, penetrated into hypoxic tumor regions to directly induce cell apoptosis. However, physiological solubility merely improves the diffusion of drug in tumor tissues, but in essence does not increase hypoxic cell uptake and drug retention in cells. Design of hypoxic-targeted prodrugs for tumor hypoxic cell accumulation would be promising for effective drug delivery in future. In summary, this study provides substantial information for guiding the design of hypoxia-targeting compounds and has broad applications for the development of hypoxia-related drug delivery strategies.

SUPPORTING INFORMATION

The Supporting Information is available free of charge at https://pubs.acs.org/doi/.

Figures of the synthetic routes of HAPs, the relationship between cell viability and the reduction potential of bioreductive groups, and the effect of H4 on cell proliferation, colony formation and body weight of mice xenografted tumor models (PDF).

ACKNOWLEDGMENTS

This work was supported by the National Natural Science Foundation of China (91959129, 31870999), the Natural Science Foundation of Tianjin (18JCYBJC40900), National Thousand Young Talents Program, and Nankai University Hundred Young Academic Leaders Program.

REFERENCES

1. Wilson, W. R.; Hay, M. P. Targeting hypoxia in cancer therapy. *Nat Rev Cancer* **2011,** *11*, (6), 393-410.
2. Liu, J. N.; Bu, W.; Shi, J. Chemical Design and Synthesis of Functionalized Probes for Imaging and Treating Tumor Hypoxia. *Chem Rev* **2017,** *117*, (9), 6160-6224.
3. Harris, A. L. Hypoxia--a key regulatory factor in tumour growth. *Nat Rev Cancer* **2002,** *2*, (1), 38-47.
4. Chang, H. Y.; Liu, H. S.; Lai, M. D.; Tsai, Y. S.; Tzai, T. S.; Cheng, H. L.; Chow, N. H. Hypoxia promotes nuclear translocation and transcriptional function in the oncogenic tyrosine kinase RON. *Cancer Res* **2014,** *74*, (16), 4549-62.
5. Sahlgren, C.; Gustafsson, M. V.; Jin, S.; Poellinger, L.; Lendahl, U. Notch signaling mediates hypoxia-induced tumor cell migration and invasion. *P Nati Acad Sci* **2008,** *105*, (17), 6392-6397.
6. Matsumoto, S.; Kishimoto, S.; Saito, K.; Takakusagi, Y.; Munasinghe, J. P.; Devasahayam, N.; Hart, C. P.; Gillies, R. J.; Mitchell, J. B.; Krishna, M. C. Metabolic and Physiologic Imaging Biomarkers of the Tumor Microenvironment Predict Treatment Outcome with Radiation or a Hypoxia-Activated Prodrug in Mice. *Cancer Res* **2018,** *78*, (14), 3783-3792.
7. Cui, D.; Huang, J.; Zhen, X.; Li, J.; Jiang, Y.; Pu, K. A Semiconducting Polymer Nano-prodrug for Hypoxia-Activated Photodynamic Cancer Therapy. *Angew Chem Int Ed* **2019,** *58*, (18), 5920-5924.
8. Yang, S.; Tang, Z.; Hu, C.; Zhang, D.; Shen, N.; Yu, H.; Chen, X. Selectively Potentiating Hypoxia Levels by Combretastatin A4 Nanomedicine: Toward Highly Enhanced Hypoxia-Activated Prodrug Tirapazamine Therapy for Metastatic Tumors. *Adv Mater* **2019,** *31*, 1805955(1-7).
9. Liang, D.; Millera, G. H.; Tranmer, G. K. Hypoxia Activated Prodrugs: Factors Influencing Design and Development. *Curr Med Chem* **2015,** *22*, 4313-4325.
10. Zhou, F.; Fu, T.; Huang, Q.; Kuai, H.; Mo, L.; Liu, H.; Wang, Q.; Peng, Y.; Han, D.; Zhao, Z.; Fang, X.; Tan, W. Hypoxia-Activated PEGylated Conditional Aptamer/Antibody for Cancer Imaging with Improved Specificity. *J Am Chem Soc* **2019,** *141*, (46), 18421−18427.

11. Denny, W. A. The role of hypoxia-activated prodrugs in cancer therapy. *Lancet Oncol* **2000,** *1*, (1), 25-29.
12. Hunter, F. W.; Wouters, B. G.; Wilson, W. R. Hypoxia-activated prodrugs: paths forward in the era of personalised medicine. *Br J Cancer* **2016,** *114*, (10), 1071-7.
13. Denny, W. A. Hypoxia-activated prodrugs in cancer therapy: progress to the clinic. *Future Oncol.* **2010,** *6*, (3), 419–428.
14. Denny, W. A. Prodrug strategies in cancer therapy. *Eu J Med Chem* **2001,** *36*, (7-8), 577–595.
15. Dragovich, P. S.; Broccatelli, F.; Chen, J.; Fan, P.; Le, H.; Mao, W.; Pillow, T. H.; Polson, A. G.; Wai, J.; Xu, Z.; Yao, H.; Zhang, D. Design, synthesis, and biological evaluation of pyrrolobenzodiazepine-containing hypoxia-activated prodrugs. *Bioorg Med Chem Lett* **2017,** *27*, (23), 5300-5304.
16. Meng, F.; Evans, J. W.; Bhupathi, D.; Banica, M.; Lan, L.; Lorente, G.; Duan, J. X.; Cai, X.; Mowday, A. M.; Guise, C. P.; Maroz, A.; Anderson, R. F.; Patterson, A. V.; Stachelek, G. C.; Glazer, P. M.; Matteucci, M. D.; Hart, C. P. Molecular and cellular pharmacology of the hypoxia-activated prodrug TH-302. *Mol Cancer Ther* **2012,** *11*, (3), 740-51.
17. Su, M.-X.; Zhang, L.-L.; Huang, Z.-J.; Shi, J.-J.; Lu, J.-J. Investigational Hypoxia-Activated Prodrugs: Making Sense of Future Development. *Curr Drug Targets* **2019,** *20*, (6), 668 - 678.
18. O'Connor, L. J.; Cazares-Korner, C.; Saha, J.; Evans, C. N.; Stratford, M. R.; Hammond, E. M.; Conway, S. J. Design, synthesis and evaluation of molecularly targeted hypoxia-activated prodrugs. *Nat Protoc* **2016,** *11*, (4), 781-94.
19. Wardman, P. Electron Transfer and Oxidative Stress as Key Factors in the Design of Drugs Selectively Active in Hypoxia. *Curr Med Chem* **2001,** *8*, (7), 739-761.
20. Hicks, K. O.; Siim, B. G.; Jaiswal, J. K.; Pruijn, F. B.; Fraser, A. M.; Patel, R.; Hogg, A.; Sarath Liyanage, H. D.; Dorie, M. J.; Martin Brown, J.; Denny, W. A.; Hay, M. P.; Wilson, W. R. Pharmacokinetic/Pharmacodynamic Modeling Identifies SN30000 and SN29751 as Tirapazamine Analogues with Improved Tissue Penetration and Hypoxic Cell Killing in Tumors. *Clin Cancer Res* **2010,** *16*, 4946-4957.
21. Dewhirst, M. W.; Secomb, T. W. Transport of drugs from blood vessels to tumour tissue. *Nat Rev Cancer* **2017,** *17*, (12), 738-750.
22. Minchinton, A. I.; Tannock, I. F. Drug penetration in solid tumours. *Nat Rev Cancer* **2006,** *6*, (8), 583–592.
23. Perche, F.; Biswas, S.; Wang, T.; Zhu, L.; Torchilin, V. P. Hypoxia-Targeted siRNA Delivery. *Angew Chem Int Ed* **2014,** *53*, (13), 3362–3366.
24. Wardman, P. Some Reactions and Properties of Nitro Radical-Anions Important in Biology and Medicine. *Environ Health Perepect* **1985,** *64*, 309-320.
25. Fu, Y.; Lai, Y.; Liu, J.; Liu, X.; You, Z.; Yang, G. Lentivirus-mediated shRNA interference of clusterin blocks proliferation, motility, invasion and cell cycle in the ovarian cancer cells. *J Ovarian Res* **2015,** *8*, 59.

26. Lv, M.; Li, S.; Luo, C.; Zhang, X.; Wang, F.; Wang, X.; Yang, J.; Liu, P.; Shen, Y.; Yang, J. Angiomotin promotes renal epithelial and carcinoma cell proliferation by retaining the nuclear YAP. *Oncotarget* **2016,** *7*, (11), 12393-12403.
27. Qian, Y.; Zhang, L.; Cai, M.; Li, H.; Xu, H.; Yang, H.; Zhao, Z.; Rhie, S. K.; Farnham, P. J.; Shi, J.; Lu, W. The prostate cancer risk variant rs55958994 regulates multiple gene expression through extreme long-range chromatin interaction to control tumor progression. *Sci Adv* **2019,** *5*, eaaw6710 (1-12).
28. Groehler, A. t.; Villalta, P. W.; Campbell, C.; Tretyakova, N. Covalent DNA-Protein Cross-Linking by Phosphoramide Mustard and Nornitrogen Mustard in Human Cells. *Chem Res Toxicol* **2016,** *29*, (2), 190-202.
29. Hales, B. F. Comparison of the Mutagenicity and Teratogenicity of Cyclophosphamide and Its Active Metabolites, 4-Hydroxycyclophosphamide, Phosphoramide Mustard, and Acrolein. *Cancer Res* **1982,** *42*, (8), 3016-3021.
30. Colvin, M.; Brundrett, R. B.; Kan, M.-N. N.; Jardine, l.; Fenselau, C. Alkylating Properties of Phosphoramide Mustard. *Cancer Res* **1976,** *36*, (3), 1121-1126.
31. Li, Z.; Gao, X.; Shi, W.; Li, X.; Ma, H. 7-((5-Nitrothiophen-2-yl)methoxy)-3H-phenoxazin-3-one as a spectroscopic off-on probe for highly sensitive and selective detection of nitroreductase. *Chem Commun (Camb)* **2013,** *49*, (52), 5859-61.
32. Chen, X.; Shen, X. Y.; Guan, E.; Liu, Y.; Qin, A.; Sun, J. Z.; Tang, B. Z. A pyridinyl-functionalized tetraphenylethylene fluorogen for specific sensing of trivalent cations. *Chem Commun (Camb)* **2013,** *49*, (15), 1503-5.
33. Fang, Y.; Liu, T.; Zou, Q.; Zhao, Y.; Wu, F. Water-soluble benzylidene cyclopentanone based photosensitizers for in vitro and in vivo antimicrobial photodynamic therapy. *Sci Rep* **2016,** *6*, 28357.
34. Nytko, K. J.; Grgic, I.; Bender, S.; Ott, J.; Guckenberger, M.; Riesterer, O.; Pruschy, M. The hypoxia-activated prodrug evofosfamide in combination with multiple regimens of radiotherapy. *Oncotarget* **2017,** *8*, (14), 23702-23712.
35. Hunter, F. W.; Young, R. J.; Shalev, Z.; Vellanki, R. N.; Wang, J.; Gu, Y.; Joshi, N.; Sreebhavan, S.; Weinreb, I.; Goldstein, D. P.; Moffat, J.; Ketela, T.; Brown, K. R.; Koritzinsky, M.; Solomon, B.; Rischin, D.; Wilson, W. R.; Wouters, B. G. Identification of P450 Oxidoreductase as a Major Determinant of Sensitivity to Hypoxia-Activated Prodrugs. *Cancer Res* **2015,** *75*, (19), 4211-23.
36. Xinglu Huang, J. Z., Seung Woo Chung, Buwei Huang, Gilad Halpert, Karina Negron, Xuanrong Sun, Jun Yang, Yumin Oh, Paul M. Hwang, Justin Hanes, Jung Soo Suk. Hypoxia-tropic Protein Nanocages for Modulation of Tumor- and Chemotherapy-Associated Hypoxia. *ACS nano* **2019,** *13*, (1), 236-247.
37. Gao, F.; Wu, J.; Gao, H.; Hu, X.; Liu, L.; Midgley, A. C.; Liu, Q.; Sun, Z.; Liu, Y.; Ding, D.; Wang, Y.; Kong, D.; Huang, X. Hypoxia-tropic nanozymes as oxygen generators for tumor-favoring theranostics. *Biomaterials* **2020,** *230*, 119635.
38. Sugahara, K. N.; Teesalu, T.; Karmali, P. P.; Kotamraju, V. R.; Agemy, L.; Greenwald, D. R.; Ruoslahti, E. Coadministration of a Tumor-Penetrating Peptide Enhances the Efficacy of Cancer Drugs. *Science* **2010,** *328*, (5981), 1031-1035.

39. Primeau, A. J. R., Augusto; Hedley, David; Lilge, Lothar; Tannock, Ian F. The Distribution of theAnticancer Drug Doxorubicin in Relation to BloodVessels in SolidTumors. *Clin Cancer Res* **2005,** *11*, (24), 8782-8788.
40. Tercel, M.; Atwell, G. J.; Yang, S.; Ashoorzadeh, A.; Stevenson, R. J.; Jane Botting, K.; Gu, Y.; Mehta, S. Y.; Denny, W. A.; Wilson, W. R.; Pruijn, F. B. Selective Treatment of Hypoxic Tumor Cells In Vivo: Phosphate Pre-Prodrugs of Nitro Analogues of the Duocarmycins. *Angew Chem Int Ed* **2011,** *50*, (11), 2606-2609.